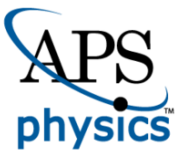

Measurement of Preheat Due to Nonlocal Electron Transport in Warm Dense Matter

K. Falk, M. Holec, C. J. Fontes, C. L. Fryer, C. W. Greeff, H. M. Johns, D. S. Montgomery, D. W. Schmidt, and M. Šmíd

Phys. Rev. Lett. **120**, 025002 — Published 10 January 2018

DOI: 10.1103/PhysRevLett.120.025002

Measurement of preheat due to nonlocal electron transport in warm dense matter

K. Falk,[1,*] M. Holec,[2,1,3,†] C. J. Fontes,[4] C. L. Fryer,[4] C. W. Greeff,[4]
H. M. Johns,[4] D. S. Montgomery,[4] D. W. Schmidt,[4] and M. Šmíd[1]

[1] *Institute of Physics of the ASCR, ELI-Beamlines, 182 21 Prague, Czech Republic*
[2] *Centre Lasers Intenses et Applications, Universite de Bordeaux-CNRS-CEA, UMR 5107, F-33405 Talence, France*
[3] *Faculty of Nuclear Sciences and Physical Engineering, Czech Technical University in Prague, Prague 1, Czech Republic*
[4] *Los Alamos National Laboratory, Los Alamos, New Mexico 87545, USA*

(Dated: December 1, 2017)

This work presents a novel approach to study electron transport in warm dense matter. It also includes the first X-ray Thomson Scattering (XRTS) measurement from low-density CH foams compressed by a strong laser-driven shock at the OMEGA laser facility. The XRTS measurement was combined with VISAR and optical pyrometry (SOP) providing a robust measurement of thermodynamic conditions in the shock. Evidence of significant preheat contributing to elevated temperatures reaching $17.5-35$ eV in shocked CH foam was measured by XRTS. These measurements were complemented by abnormally high shock velocities observed by VISAR and early emission seen by SOP. These results were compared to radiation hydrodynamics simulations that include first-principles treatment of nonlocal electron transport in WDM with excellent agreement. Additional simulations confirmed that the X-ray contribution to this preheat is negligible.

PACS numbers: 62.50.-p, 64.30.-t, 61.20.-p, 52.27.Gr

The thermodynamic properties and dynamic behavior of materials at extreme conditions of high energy density (HED) states are relevant to many astrophysical objects [1] and Inertial Confinement Fusion (ICF) [2]. A particularly problematic state is Warm Dense Matter (WDM) defined by moderately high temperatures of 0.1–100 eV, solid densities, and pressures above 1 Mbar. Under such conditions, ions are strongly correlated and the electron population is partially or fully degenerate making the theoretical description of WDM very challenging. Thus robust measurements of the equation of state (EOS), structure and transport properties of WDM are crucial to the understanding of many processes in the formation and structure of astrophysical objects such as Jovian planets or white dwarfs as well as the dynamics of the ICF implosions [3, 4]. Heat and radiative transport through various layers influences the layer structure and convection of astrophysical objects, and electrical conductivity strongly affects magnetic fields generated by planetary core dynamos [5]. Alternative fusion schemes such as fast ignition rely on heating of fusion targets by energy deposition of electrons [6, 7]. Preheat of target components due to X-rays and energetic particles in laser-driven HED systems is a well-known problem causing changes in initial conditions and multiple hydrodynamic instabilities in EOS and ICF experiments [9, 10]. Specifically electron transport in dense laser-heated plasmas holds the key to understanding many fundamental questions [11].

Despite great challenges, much progress has been made in the theoretical description of structure, EOS as well as transport properties of WDM [12, 13]. Examples of remarkable work include *ab initio* quantum molecular dynamics (QMD) simulations obtaining thermal conductivity of warm dense hydrogen [14], resistivity saturation in warm dense Al [15], and charged particle stopping powers, and transport has been described both by using pure theory as well as with molecular dynamics (MD) simulations [16, 17]. The concept of nonlocal electron transport modeling in hydrodynamic simulations was first introduced to compute the delocalization strategy of the classical diffusion approach [18]. This model had a great impact and led to a consequent improvement of the hydrodynamic simulations in experimental data prediction. It was not until much later that the first attempt to include a real nonlocal transport model retaining on a first-principles approach based on kinetics came and addressed the necessity of using the proper physics [19].

In this article we present our recent work where we utilize a platform previously developed for direct measurements of temperature and shock velocity in order to study nonlocal electron transport in WDM [20]. The analysis of our data showed that the stronger drive used in this experiment caused nonlocal electrons to preheat the CH sample. A detailed theoretical study confirmed that this effect leads to observed shock velocities and temperatures well above those expected without preheat. In past years, there have been some experiments measuring the transport properties of electrons in dense plasmas [24] and radiation transport in standard materials [25, 26], however no full characterization including complete measurement of plasma conditions with *in situ* measurements of transport coefficients has been achieved to date. A newly established diagnostic technique of X-ray Thomson

*Email: falk@fzu.cz
†Email: milan.holec@u-bordeaux.fr

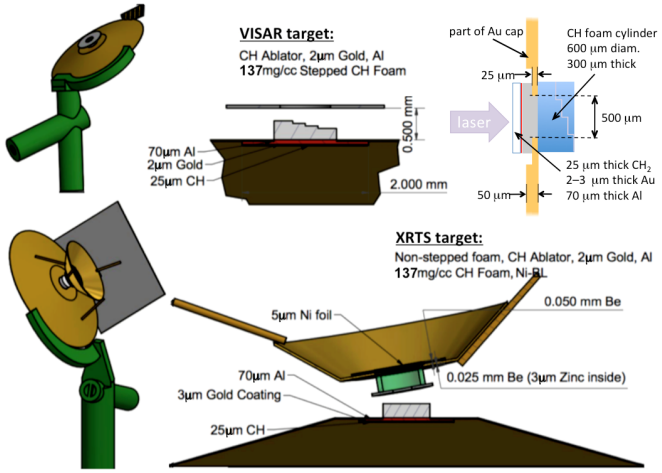

FIG. 1: A schematic of the targets. The driven target sits inside the larger Au cone and consists of a plastic ablator, Au radiation shield, Al pusher and C_8H_8 foam. The XRTS target also includes a second smaller cone containing Ni backlighter and Ta slit used to collimate the X-rays. Laser beams illuminate the ablator from inside of each cone. The VISAR target is identical, but has no backlighter and includes a four steps on the back side of the foam. Additional Ta shielding was used to restrict the view of VISAR and XRTS.

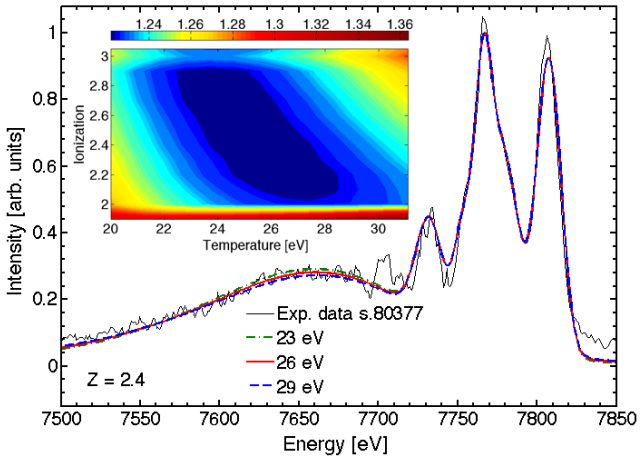

FIG. 2: X-ray scattering data from shocked C_8H_8 polystyrene foam. The best fit conditions were $T_e = 26 \pm 3$ eV, $n_e = 8.43 \times 10^{22}$ cm^{-3} and $Z \sim 2.4$. The error bars were estimated from a χ^2 fit (inserted image).

Scattering (XRTS) opens a novel path towards studying structure and transport properties in WDM [27]. XRTS is capable of obtaining information about temperature, density, ionization state as well as microscopic properties of dense plasmas. If combined with other diagnostics such as velocity interferometry (VISAR), streaked optical pyrometry (SOP) or radiography, it can then provide a comprehensive measurement of thermodynamic properties of WDM [20, 28].

The experiment was carried out at the OMEGA laser facility at the University of Rochester [30]. The WDM conditions were created by a single shock driven by laser ablation from the surface of the target. Fifteen of the laser beams were overlapped to give a $\sim 7\times10^{14}$ W/cm^2 *square* drive with 2 ns duration. The drive beams were frequency-tripled to give λ=351 nm output and their spatial profile was smoothed with distributed phase plates [31]. The targets were planar layered structures consisting of 25 μm plastic (CH) ablator, 2–3 μm Au coating used to shield X-ray radiation created at the critical surface of the laser-plasma interaction, 70 μm Al pusher and 300 μm of C_8H_8 polystyrene foam. The density of the foam, measured by soft X-ray transmission at 5.4 keV (Cr K-α source), was found to be 137.27±3.48 mg/cm^3 [32]. The polystyrene foam was made with the Hipe process and the pore sizes were measured with a scanning electron microscope (SEM) obtaining the average pore diameter of 1.26 μm. The schematics of the target layouts are shown in Fig. 1.

The thermodynamic conditions in the shockwave traveling through the C_8H_8 foam were studied with a number of diagnostics developed for the platform including VISAR, SOP and XRTS [20]. The XRTS and VISAR/SOP measurements were carried separately due to geometrical constraints, but the laser drive was kept the same in both cases and the platform has shown good shot-to-shot reproducibility. The shock velocity was measured by a two interferometer VISAR system operating at 532 nm by detecting shock breakout timing across four 40 μm steps manufactured on the back side of the foam on VISAR targets [33]. Supporting measurements of shock breakout timing were obtained from direct emission observed by the SOP system [34]. The average shock velocities at the time of break out were found to be 57.8±3.8 km/s, 64.0±4.9 km/s and 67.5±5.0 km/s respectively for different shots. These shock velocities were rapidly decaying with significant slowing of the shockwaves. SOP observed early emission that came $\sim$ 1 ns before the VISAR signal confirming the presence of preheat in the foam.

The temperature was obtained from analytical fits to the broadening of the inelastic Compton feature in the XRTS spectra in the non-collective geometry [27]. The X-ray probe used for XRTS was He-α line emission at 7.8 keV generated by ten 1 ns backlighter beams with intensity of 2–3$\times10^{15}$ W/cm^2 focused onto 5 μm thick Ni foil [35]. The X-rays were then collimated by a 200 μm diameter Ta slit placed 500 μm away from the studied carbon sample, defining the scattering angle at 95° ± 5°. The scattering signal was detected by spatially and spectrally resolved Imaging X-ray Thomson Spectrometer (IXTS) which utilizes a toroidally curved Ge (220) crystal coupled with a deep-depletion CCD camera [36]. The XRS code was used to compute analytical fits to the scattering spectra [37–39].

The XRS fits were calculated using measured source spectrum and varied input conditions including the elec-

TABLE I: Summary of XRTS results.

Shot no. - lineout	XRTS delay	Temperature (T_e)	Z
80375	5.5 ns	17.5 ± 2.5 eV	2.5
80373 (lower)	6.0 ns	24.5 ± 4.5 eV	2.2
80373 (upper)	6.0 ns	27.0 ± 2.5 eV	2.9
80377 (lower)	6.0 ns	23.0 ± 3.0 eV	2.8
80377 (middle)	6.0 ns	25.5 ± 2.5 eV	2.8
80377 (upper)	6.0 ns	26.0 ± 3.0 eV	2.4
80376	6.5 ns	35.0 ± 5.0 eV	2.2

tron temperature T_e, density n_e and ionization state Z and compared with experimental data as shown in Fig. 2. The temperature in each sample was obtained from the best fit to the data and the error bars were estimated using χ^2 fitting and matched to one standard deviation of the noise in the Compton peak, see insert in Fig. 2. Some XRTS spectra had some contamination by direct emission from blow off Ni plasma, which was possible to be reduced from the data thanks to the spatial resolution of the IXTS instrument. In the case of shots 80373 and 80377 multiple lineouts could be retrieved from the data that corresponded to slightly different times during the shock wave evolution, i.e. *upper* lineout corresponds to an later time. A clear trend is seen in the data, the shock temperature increases with time. The XRTS results are summarized in Table 1.

The experimental results were first compared to EOS tables including SESAME 7593 [40] and FPEOS [41] in Hugoniot calculations confirming that CH temperatures in the range of 20–30 eV would require higher shock velocities. We tested this with simulations carried out by the high-energy density code Cassio developed at LANL combining the Radiation adaptive grid Eulerian (RAGE) code [42] coupled with an implicit Monte Carlo treatment [43]. For these calculations, we used a 72 energy group structure, using Rosseland binning for the SESAME opacities [44]. Although the plastic ablator region heats up beyond 100 eV, the simulations show that no X-rays leak through to the foam target and there is no significant X-ray preheat. No explicit treatment of electron transport is included in the code. With no preheat included the shock velocities and temperatures in the simulation are lower than observed in the experiment. By introducing an artificial preheat of 1–10 eV (assuming the electrons stream through the target, heating uniformly), the simulation results better match the higher temperatures, but never reproduce the observed shock velocities. The effect of possible preheat was further studied by using spectral simulations. First, the radiation emission of CH pusher during the laser irradiation ($T = 2$ keV, $\rho = 7\times10^{-3}$ g/cm^3, $L = 750$ μm) in the range $0.1-10$ keV was modeled by using the Flychk code and this radiation was multiplied by the transmission of Au and Al layers [45, 46]. It was found that a flux of only 19 J/cm^3 was absorbed in the foam. Another possible source of preheat is the heated Au radiation shield ($T = 35$ eV, $\rho = 1.7$ g/cm^3, $L = 30$ μm). This was evaluated by a similar approach and it was found that < 110 J/cm^3 would be absorbed in the foam.

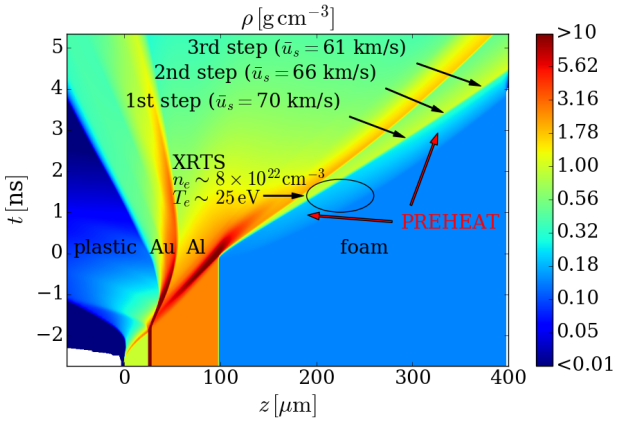

FIG. 3: Hydrodynamic simulation of a laser driven shock with the PETE code. The position of the propagating shock can be seen, where the shock velocities corresponding to the breakout times at the three steps on the rear side of the target are shown. The preheat due to nonlocal electrons can be observed and the corresponding thermodynamic conditions are in excellent agreement with the elevated temperature measured by XRTS.

In order to study the contribution of the nonlocal electron transport to the observed preheat we used the Plasma Euler and Transport Equations Hydro code (PETE), which is a Lagrangian fluid model [21]. In PETE, the plasma fluid (ions) is modeled by Euler equations, while the population of free electrons relies on the first-principles based kinetic model represented by the Bhatnagar-Gross-Krook (BGK) transport equation [22]. Such a treatment allows us to describe the nonlocal transport of electrons with respect to their mean free path (mfp), before being thermalized within the plasma fluid, thus providing the transport of energy. The results of the Omega shockwave simulations in 1D planar geometry are shown in Fig. 3. The propagating shock in the foam layer can be recognized by a set of arrows, which point to the sequence of positions of three steps manufactured on the back side of the target and show a very good agreement between simulated and experimentally measured shock velocities and the strong decay in time. This is a natural consequence of the nonlocal BGK electron transport, which leads to a higher temperature when the shock propagates. We were unable to reproduce this behavior with the classical heat conduction model [23]. In every time step, the foam shockwave exhibits finite preheat. Its maximum thickness can be seen at the position $z = 250$ μm in Fig. 3. Physically relevant conditions for such a preheat to occur are high temperature or, more precisely, a sufficiently high Knudsen number Kn = mfp/L, where L is the temperature length scale. If we compare the jump along the shock of

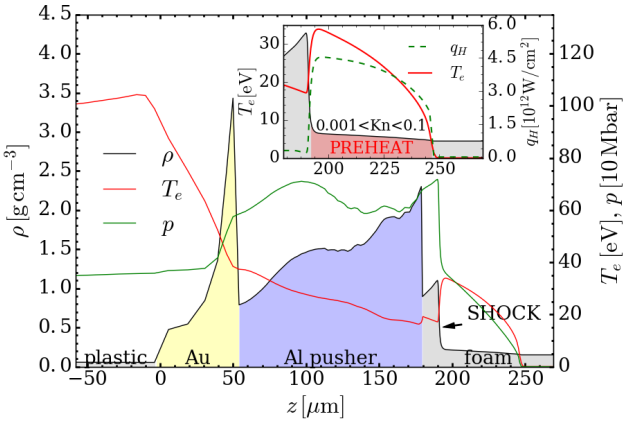

FIG. 4: The shock propagating in the foam layer can be seen in the hydrodynamic simulation profiles of density ρ, electron temperature T_e, and pressure p corresponding to the time of XRTS measurement in Fig. 3. The preheat zone is highlighted in the inset further accompanied by the profile of electron energy flux density q_H. Since the Knudsen number Kn within the highlighted zone reaches a high value 0.1 (diffusive limit 0.001), the nonlocal electron transport becomes significant ($q_H \sim u(E+p)$), thus forming the preheat.

the electron energy flux density q_h to the hydrodynamic energy flux density $u(E+p)$, where u is fluid velocity, E total energy density of plasma, and p total pressure, we find that $\Delta q_h = -0.16\,\Delta u(E+p)$, which confirms the importance of the nonlocal transport in the shock dynamics. It also qualitatively describes that we are in an off-Hugoniot regime. We have performed the Hugoniot jump condition analysis and the simulated shock velocity is in excellent agreement in every moment of the shock propagation. Corresponding plasma quantities are pictured in Fig. 4, where the inset corresponds to the XRTS region highlighted in Fig. 3 and the simulated thermodynamic conditions are again in a very good agreement with experimental data shown in Fig. 2 and Table 1. The highly localized increase in q_H along the shock clarifies that the nonlocal electrons originate from a thin post-shock layer and are thermalized within the finite preheat region. The effect of a consequent heating gives the absorbed flux 2.7×10^6 J/cm^3, which surpasses the calculated heating effect of X-rays by several orders of magnitude.

In conclusion, this experiment demonstrated the first measurement of nonlocal transport of electrons through WDM causing significant preheat in the target. Direct measurements of temperature and shock velocity by independent diagnostics including XRTS, VISAR and SOP were matched with the results from PETE simulations that include the first-principles based BGK model providing the nonlocal transport of free electrons. According to these simulations, the nonlocal electron transport allows additional transport of energy apart from the hydrodynamic shock resulting in increased temperature, pressure, and consequently, higher shock velocity. Additional simulations including the Flychk and Cassio codes confirmed that the X-ray contribution to this preheat is negligible compared to the heating effect due to nonlocal electrons.

These findings enable bench-marking of electron conduction models in conditions relevant to ICF, such as those employed in the modeling of experiments performed at the National Ignition Facility (NIF), and convection phenomena in white dwarfs [47].

The authors would like to acknowledge the work of the LANL target fabrication group, the OMEGA experimental team, P. A. Keiter and S. R. Klein for their work on the IXTS, C. E. Starrett and D. Saumon for useful discussions. This research was supported by the US DOE/NNSA under contract number DE-AC52-06NA25396 and by the project ELI - Extreme Light Infrastructure (CZ.02.1.01/0.0/0.0/15 008/0000162) from European Regional Development Fund.

[1] S. Lebedev *High Energy Density Laboratory Astrophysics*, Springer (2007).
[2] R. L. McCrory *et al.*, Nucl. Fusion **45**, S283 (2005).
[3] T. Guillot, Science **286**, 72-77 (1999).
[4] O. Hurricane *et al.*, Nature 506, 343 (2014).
[5] P. Olson, Science **342**, 431 (2013).
[6] S. Humphries Jr., Nucl. Fusion **20**, 1549 (1980).
[7] M. Tabak *et al.*, Phys. Plasmas **1**, 1626 (1994).
[8] A. Benuzzi *et al.*, Phys. Plasmas **5**, 6 (1998).
[9] C. A. Di Stefano *et al.*, Phys. Rev. E **95**, 023202 (2017).
[10] R. S. McWilliams *et al.*, Science **338**, 1330 (2012).
[11] V. N. Goncharov *et al.*, Phys. Plasmas **13**, 012702 (2006).
[12] K. P. Driver and B.Militzer, Phys. Rev. Lett. **108**, 115502 (2012).
[13] D. Saumon, C. E. Starrett, J. Kress, J. Clerouin, HEDP **8**, 150 (2012).
[14] V. Recoules *et al.*, Phys. Rev. Lett. **102**, 075002 (2009).
[15] G. Faussurier and C. Blancard, Phys. Rev. E **91**, 013105 (2015).
[16] C. K. Li and R. D. Petrasso, Phys. Rev. Lett. **70**, 3059 (1993); **114**, 199901(E) (2015).
[17] P. E. Grabowski *et al.*, Phys. Rev. Lett. **111**, 215002 (2013).
[18] J. F. Luciani, P. Mora and J. Virmont, Phys. Rev. Lett. **51**, 1664 (1983).
[19] W. Manheimer, D. Colombant and V. Goncharov, Phys. Plasmas **15**, 083103 (2008).
[20] K. Falk, *et al.*, Phys. Rev. Lett. **112**, 155003 (2014).
[21] M. Holec *et al.*, Int. J. Numer. Meth. Fluids, DOI: 10.1002/fld.4288 (2016).
[22] P. Bhatnagar, E. Gross, and M. Krook, Phys. Rev. **94**, 511 (1954).
[23] J. L. Spitzer and R. Harm, Phys. Rev. **89**, 977 (1954).
[24] J. Pasley *et al.*, Phys. Plasmas **14**, 120701 (2007).

[25] E. Falize, C. Michaut, and S. Bouquet, Astrophys. J. **730**, 96 (2011).
[26] P. A. Rosen *et al.*, Astrophys. Space Sci. **322**, 101 (2009).
[27] S. H. Glenzer and R. Redmer, Rev. Mod. Phys. **81**, 1625 (2009).
[28] K. Falk, *et al.*, Phys. Plasmas **21**, 056309 (2014).
[29] K. Falk *et al.*, Phys. Rev E. **87**, 043112 (2013).
[30] T. R. Boehly *et al.* , Opt. Commun. **133**, 495 (1997).
[31] S. P. Regan *et al.*, J. Opt. Soc. Am. B **22**, 998 (2005).
[32] N. E. Lanier, C. Hamilton, and J. M. Taccetti, Rev. Sci. Instrum. **83**, 10E520 (2012)
[33] P. M. Celliers *et al.*, Rev. Sci. Instrum., **75**, 4916 (2004).
[34] M. C. Gregor *et al.*, Rev. Sci. Instrum. **87**, 114903 (2016).
[35] J. Workman and G. A. Kyrala, Proc. SPIE **4504**, 168-179 (2001).
[36] E. J. Gamboa *et al.*, Rev. Sci. Instrum. **83**, 10E108 (2012).
[37] G. Gregori *et al.*, Phys. Plasmas **17**, 052709 (2010).
[38] G. Gregori and D. O. Gericke, Phys. Plasmas **16**, 056306 (2009).
[39] D. O. Gericke, J. Vorberger, K. Wünsch, and G. Gregori, Phys. Rev. E **81**, 065401(R) (2010).
[40] S. P. Lyon and J. D. Johnson, Los Alamos National Laboratory Report LA-UR-92-3407 (1992).
[41] S. X. Hu *et al.*, Phys. Rev. E **92**, 43104 (2015).
[42] M. Gittings *et al.*, CS&D **1**, 015005, 63, (2008).
[43] T. J. Urbatsch and T. M. Evans, Los Alamos National Laboratory Report LA-14195-MS (2005).
[44] J. Colgan *et al.*, Astrophys. J. **817**, 116 (2016).
[45] H.-K. Chung *et al.*, High Energy Density Physics **1**, 3 (2005).
[46] B. L. Henke, E. M. Gullikson, and J. C. Davis, Atomic Data and Nuclear Data Tables **54**, 181-342 (1993).
[47] G. Fontaine, P. Brassard and P. Bergeron, PASP **113**, 409 (2001).